Activation of *Notch* and *Myc* Signaling via B-cell–Restricted Depletion of *Dnmt3a* Generates a Consistent Murine Model of Chronic Lymphocytic Leukemia

Anat Biran[1,2], Shanye Yin[1,2], Helene Kretzmer[3], Elisa ten Hacken[1,2], Salma Parvin[1,2], Fabienne Lucas[4], Mohamed Uduman[5], Catherine Gutierrez[1,2], Nathan Dangle[1], Leah Billington[1], Fara Faye Regis[1], Laura Z. Rassenti[6], Arman Mohammad[7,8], Gabriela Brunsting Hoffmann[1], Kristen Stevenson[8], Mei Zheng[4], Elizabeth Witten[1], Stacey M. Fernandes[1], Eugen Tausch[9], Clare Sun[10], Stephan Stilgenbauer[9], Jennifer R. Brown[1,2], Thomas J. Kipps[6], John C. Aster[4], Andreas Gnirke[7], Donna S. Neuberg[8], Anthony Letai[1,2], Lili Wang[11], Ruben D. Carrasco[2,4,12], Alexander Meissner[3,7,13], and Catherine J. Wu[1,2,7]

ABSTRACT

Chronic lymphocytic leukemia (CLL) is characterized by disordered DNA methylation, suggesting these epigenetic changes might play a critical role in disease onset and progression. The methyltransferase *DNMT3A* is a key regulator of DNA methylation. Although *DNMT3A* somatic mutations in CLL are rare, we found that low *DNMT3A* expression is associated with more aggressive disease. A conditional knockout mouse model showed that homozygous depletion of *Dnmt3a* from B cells results in the development of CLL with 100% penetrance at a median age of onset of 5.3 months, and heterozygous *Dnmt3a* depletion yields a disease penetrance of 89% with a median onset at 18.5 months, confirming its role as a haploinsufficient tumor suppressor. B1a cells were confirmed as the cell of origin of disease in this model, and *Dnmt3a* depletion resulted in focal hypomethylation and activation of *Notch* and *Myc* signaling. Amplification of chromosome 15 containing the *Myc* gene was detected in all CLL mice tested, and infiltration of high-*Myc*–expressing CLL cells in the spleen was observed. Notably, hyperactivation of *Notch* and *Myc* signaling was exclusively observed in the *Dnmt3a* CLL mice, but not in three other CLL mouse models tested (*Sf3b1-Atm*, *Ikzf3*, and *MDR*), and *Dnmt3a*-depleted CLL were sensitive to pharmacologic inhibition of *Notch* signaling *in vitro* and *in vivo*. Consistent with these findings, human CLL samples with lower *DNMT3A* expression were more sensitive to *Notch* inhibition than those with higher *DNMT3A* expression. Altogether, these results suggest that *Dnmt3a* depletion induces CLL that is highly dependent on activation of *Notch* and *Myc* signaling.

Significance: Loss of *DNMT3A* expression is a driving event in CLL and is associated with aggressive disease, activation of *Notch* and *Myc* signaling, and enhanced sensitivity to *Notch* inhibition.

Introduction

Recent large-scale cancer sequencing studies performed over the past decade have revealed a myriad of candidate genetic lesions that drive malignancies, however, the functional effects of these newly somatic mutations have remained largely unknown (1, 2). For chronic lymphocytic leukemia (CLL), growing efforts to address this challenge have yielded the recent generation of *in vivo* models engineered to recapitulate the B-cell–restricted expression of novel putative genetic drivers. These studies have confirmed the CLL-driving roles of alterations such as mutated *SF3B1* in conjunction with *ATM* deletion, and hotspot mutations in *IKZF3*, and altogether highlight the common and diverse mechanisms underlying CLL pathogenesis [i.e., dysregulation of B-cell receptor (BCR) signaling; refs. 3, 4].

In addition to genetic lesions, recent studies have further highlighted the role of epigenetic aberrations in cancer development (5, 6). DNA methylation is one of the most well studied epigenetic abnormalities in human cancers and dysregulation of DNA methylation can lead to genome instability and the silencing of tumor suppressor genes (7, 8). In line with this notion, previous studies have revealed that CLL is characterized by prominent locally disordered methylation disorder (9, 10). These characteristic changes in DNA methylation suggest a critical role in the onset and progression of CLL (10–12). In mammalian cells, DNA methylation is dynamically established by the DNA methyltransferase 3 (*DNMT3*) family of *de novo* methyltransferases *DNMT3A* and *DNMT3B* and sustained by the maintenance methyltransferase *DNMT1* (13). Previous studies suggested that

[1]Department of Medical Oncology, Dana-Farber Cancer Institute, Boston, Massachusetts. [2]Harvard Medical School, Boston, Massachusetts. [3]Department of Genome Regulation, Max Planck Institute for Molecular Genetics, Berlin, Germany. [4]Department of Pathology, Brigham and Women's Hospital, Harvard Medical School, Boston, Massachusetts. [5]Center for Immuno-Oncology, Dana-Farber Cancer Institute, Harvard Medical School, Boston, Massachusetts. [6]Moores Cancer Center, University of California San Diego Health, La Jolla, California. [7]Broad Institute of MIT and Harvard, Cambridge, Massachusetts. [8]Department of Data Science, Dana-Farber Cancer Institute, Harvard Medical School, Boston, Massachusetts. [9]Department of Internal Medicine III, Ulm University, Ulm, Germany. [10]Hematology Branch, National Heart, Lung, and Blood Institute, National Institutes of Health, Bethesda, Maryland. [11]Department of Systems Biology, Beckman Research Institute, City of Hope National Comprehensive Cancer Center, Monrovia, California. [12]Department of Oncologic Pathology, Dana-Farber Cancer Institute, Harvard Medical School, Boston, Massachusetts. [13]Department of Stem Cell and Regenerative Biology, Harvard University, Cambridge, Massachusetts.

Note: Supplementary data for this article are available at Cancer Research Online (http://cancerres.aacrjournals.org/).

A. Biran and S. Yin contributed equally to this article.

Corresponding Author: Catherine J. Wu, Department of Medical Oncology, Dana-Farber Cancer Institute, 450 Brookline Avenue, Boston, MA 02215. Phone: 617-632-5943; E-mail: cwu@partners.org

Cancer Res 2021;81:6117–30

doi: 10.1158/0008-5472.CAN-21-1273

alterations in DNA methylation/demethylation intermediates were closely linked to clinical outcomes in CLL (14).

Although mutations of *DNMT3A* are rarely observed in CLL, we demonstrate herein that low *DNMT3A* expression is associated with more aggressive disease through the analysis of two independent CLL cohorts. To explore the hypothesis that loss of *DNMT3A* expression functionally contributes to CLL pathogenesis, we engineered a conditional knockout (KO) mouse model with B-cell–restricted deletion of *Dnmt3a* through intercrossing with the *CD19*-Cre recombinase (Cre) system. Strikingly, homozygous *Dnmt3a* depletion in B cells resulted in the development of CLL with 100% penetrance at a median age of onset of 5.3 months, and heterozygous *Dnmt3a* depletion yielded a disease penetrance of 89% with a median onset at 18.5 months, confirming its role as a haploinsufficient tumor suppressor. Distinct from other existing CLL models tested (i.e., *Sf3b1-Atm*, *Ikzf3*, and *MDR*; refs. 3, 4, 15), we observed selective activation of *Notch* and *Myc* signaling, but not BCR signaling, and sensitivity to Notch inhibition, supporting this line as a *Notch*-driven mouse model of CLL.

Materials and Methods

Animals

All animals were housed at Dana-Farber Cancer Institute (DFCI). All animal procedures were completed in accordance with the Guidelines for the Care and Use of Laboratory Animals and were approved by the Institutional Animal Care and Use Committees at DFCI (protocol no.: 07–068; 12–004). *Dnmt3a*-floxed mice were gifted from Dr. Ross Levine [Memorial Sloan Kettering Cancer Center (MSKCC); ref. 16]. *Cd19*-Cre$^{+/-}$ mice were obtained from The Jackson Laboratory. *Dnmt3a*-floxed mice were intercrossed with *Cd19*-Cre mice to generate *Cd19*-Cre *Dnmt3a*-floxed C57BL/6J mice.

CLL patient samples

Heparinized blood samples were obtained from healthy donors (HD) and patients enrolled on clinical research protocols with informed consent. The study was conducted in accordance with the ethical guidelines approved by the Human Subjects Protection Committees of DFCI; by the University of California San Diego (UCSD); by the NIH National Heart, Lung, and Blood Institute; and by the Department of Internal Medicine III at Ulm University, Germany. Peripheral blood mononuclear cells (PBMC) from normal donors and patients with CLL were isolated by Ficoll/Hypaque density gradient centrifugation. CD19$^+$ B cells from normal volunteers were isolated by immunomagnetic selection (Miltenyi Biotec). PBMCs were used fresh or cryopreserved in FBS with 10% DMSO and stored in vapor-phase liquid nitrogen until the time of analysis.

Flow cytometry

To monitor disease progression, 50 μL of blood was collected from mice via submandibular bleeds into EDTA-containing tubes. Erythrocyte lysis was achieved by incubating the blood in 1 mL of ACK buffer for 5 minutes and then washing with PBS supplemented with 2% FCS and 2 mmol/L EDTA. The cells were then stained with a cocktail of antibodies as described in Supplementary Materials and Methods for 20 minutes at 4°C. Cells were then washed and analyzed (BD LSRFortessa cell analyzer). For flow cytometric evaluation of specific cell surface markers, erythrocyte lysed single-cell suspensions prepared from spleen, bone marrow (BM), and peritoneal cavity were washed with PBS supplemented with 2% FCS and 2 mmol/L EDTA and then incubated with antibodies for 20 minutes. Splenic marginal and follicular B-cell populations were stained with a panel of antibodies as described in Supplementary Materials and Methods. All analyses of splenic and BM B cells were performed using mice of 8 to 12 weeks old, while that of B cells from the peritoneal cavity were from mice of 4 to 6 weeks of age. To analyze germinal center generation, mice of 8 to 12 weeks of age were immunized intraperitoneally with 10^9 sheep red blood cells (Immunoresearch) in 150 μL of PBS. Spleens were collected 10 days after immunization and analyzed by flow cytometry to quantify germinal center B cells using a panel of antibodies as described in Supplementary Materials and Methods. To assess proliferation of B1a cells, cells isolated from the peritoneal cavity of 8- to 12-week-old *Cd19*-Cre$^{+/-}$ or *Cd19*-Cre$^{+/-}$*Dnmt3a*$^{fl/fl}$ animals, were stained with the CellTrace CFSE Cell Proliferation Kit (Thermo Fisher Scientific) according to the manufacturer's protocol and injected intraperitoneally into irradiated immunodeficient recipients [10-week-old NOD/SCID gamma (NSG) mice]. Eleven days following injection, recipient mice were euthanized, and peritoneal fluid was collected and a panel of antibodies as described in Supplementary Materials and Methods. CD11b$^+$ B1a cells were analyzed for carboxyfluorescein diacetate succinimidyl ester (CFSE) intensity by flow cytometry.

IHC

For IHC staining, spleens were fixed in 10% buffered neutral formalin overnight followed by 70% ethanol until the tissues were processed. Spleens were then paraffin-embedded and sectioned into 20 μm for staining. Bones were fixed in 10% buffered neutral formalin overnight followed by 2 hours of 70% ethanol until the tissues were processed. Hematoxylin and eosin staining, as well as PAX5 and CD5 immunostaining were performed on the sections using standard procedures. MYC IHC was performed on the Leica Bond III automated staining platform using the Leica Biosystems.

LSK, B1a, and CLL transfer experiments

Transfer of HSC

Seven- to twelve-week-old female or male CD45.2$^+$ *Cd19*-Cre$^{+/-}$*Dnmt3a*$^{fl/fl}$ mice were used as donors. Femurs, tibias, hips, and spines were isolated from donor mice, crushed, and ACK-lysed. Cells were enriched with anti-CD117 microbeads (Miltenyi Biotec) and then sorted to collect LSK (lineage$^-$ Sca-1$^+$ c-Kit$^+$) cells using a panel of antibodies as described in Supplementary Materials and Methods.

Transfer of B1a cells

Six- to eight-week-old female or male *Cd19*-Cre$^{+/-}$ or *Cd19*-Cre$^{+/-}$*Dnmt3a*$^{fl/fl}$ mice were used as donors. B1a cells from the peritoneal cavity were sorted and injected intraperitoneally into irradiated Cd45.1$^+$ recipients, cells from of 1 donor mouse (50,000–100,000 cells) per 1 recipient mouse for total of 5 donors per genotype.

Transplantation of CLL cells

Five million splenocytes from *Cd19*-Cre$^{+/-}$*Dnmt3a*$^{fl/fl}$ were resuspended in 100 microliters PBS and injected intravenously into 8- to 15-week-old NSG mice. Overall, CLL cells from 5 different donors were transplanted into recipient mice. Disease burden in the peripheral blood, spleen, and BM was evaluated by flow cytometry and IHC.

BCR stimulation, Notch stimulation, and immunoblotting analysis

For analysis of BCR signaling transduction, purified splenic B cells (3×10^6) or splenic CLL cells were stimulated in 1 mL RPMI 1640 medium (Life Technologies) supplemented with 10% FCS, and 1%

penicillin/streptomycin in the presence of 10 μg/mL goat anti-mouse IgM (Southern Biotech) for 5 or 15 minutes at 37°C. Cells were harvested, washed twice with cold PBS, and lysed for 30 minutes on ice with RIPA buffer (Boston Bioproducts) supplemented with a protease inhibitor mix (1 tablet in 10 mL RIPA buffer; Roche) and PhosSTOP (Sigma Aldrich) according to manufacturer's protocol. Cell debris was removed by centrifugation at 10,000 per g for 15 minutes, followed by protein quantification using Pierce BCA protein assay kit (Thermo Scientific). Cell extracts were fractionated by SDS-PAGE and transferred to Immun-Blot PVDF or nitrocellulose membranes (Biorad). Membranes were stained overnight at 4°C with primary antibodies and appropriate secondary antibodies, e.g., horseradish peroxidase–coupled goat anti-rabbit and goat anti-mouse antibodies (Rockland Immunochemicals Inc). The bands were visualized by using a Biorad ChemiDoc touch imaging system. Antibodies are described in Supplementary Materials and Methods. Western blot quantification was performed using imageJ (RRID:SCR_003070).

BH3 profiling

BH3 profiling was performed as described previously (17). Experiments were performed using B cells from the spleen and peritoneal cavity of 2- to 3-month-old *Cd19*-Cre$^{+/-}$ or *Cd19*-Cre$^{+/-}$*Dnmt3a*$^{fl/fl}$, immunomagnetically isolated (B-cell Isolation Kit, Miltenyi Biotec). B cells from the peritoneal cavity were pooled together to increase total cell number. Cells were suspended in MEB2 buffer (150 mmol/L mannitol, 10 mmol/L HEPES-KOH pH 7.5, 150 mmol/L KCl, 1 mmol/L EGTA, 1 mmol/L EDTA, 0.1% BSA, 5 mmol/L succinate). Cells were added to a 384-well plate and incubated at 25°C for 60 minutes combined with different BH3 peptides in 0.001% digitonin for permeabilization. Cell were fixed with 4% formaldehyde for 10 minutes at room temperature followed by neutralization by adding N2 buffer (1.7 M Tris base, 1.25 M glycine, pH 9.1). Cells were stained overnight at 4°C with Hoechst 33342 (H3570, Invitrogen) and anti–cytochrome *c*–Alexa Fluor 488 (6H2.B4/612308) and analyzed using an Intellicyt iQue flow cytometer to determine the rate of loss of cytochrome c in response to each BH3 peptide. Splenic and peritoneal cavity cells were also stained with CD19, CD11b, and CD5 antibodies and gated for B2 cells (CD19$^+$) or CD11b$^+$ B1a cells (CD19$^+$;CD5$^+$; CD11b$^+$). Assays were generally conducted in triplicate. DMSO and alamethicin were used as negative and positive controls for cytochrome c release.

RNA collection

RNA extraction was performed on sorted splenic B cells or peritoneal cavity B1a cells from young, disease-free 4- to 6-week-old mice and from CLL cells isolated from the spleens of diseased mice and sorted to collect B220$^+$CD5$^+$IgK$^+$ cells. Total RNA was extracted using Qiagen RNAeasy kit or Qiagen RNAeasy micro kit with on-column DNase treatment (Qiagen).

In vitro drug treatment

CLL cells from different genetic CLL mouse models (3, 4, 15) were resuspended in RPMI 1640 medium supplemented with 10% FBS and cultured in 96-well tissue culture plates (50,000 cells/100 μL). Cells were treated with indicated concentrations of the BCL2 inhibitor ABT-199, BTK inhibitor ibrutinib, *Notch* signaling inhibitor daptomycin (DAPT), and Wnt signaling inhibitor LGK-974. After incubation for 24 hours at 37°C with 5% CO_2, cell viability was measured by CellTiter-Glo Luminescent Assay and normalized by cells treated with the DMSO vehicle control. Human primary CLL cells were plated at 2 million/mL in complete RPMI and exposed to 50 mmol/L DAPT, 1 nmol/L venetoclax or 1 μmol/L ibrutinib overnight, followed by CellTiter-Glo assessment of cellular viability, assessed in technical triplicates. OP9 and OP9-DLL1 were kindly provided by J.C. Aster (Brigham and Women's Hospital), were seeded in 48-well plates (250K stromal cells per well) 16 hours prior to incubation with samples, and then drug treatments were performed as above.

In vivo drug treatment

Transplantation studies were performed on 8- to 12-week-old immunodeficient recipient NSG mice using viably cryopreserved splenocytes from *Dnmt3a*$^{fl/fl}$ CLL animals. Five million CLL cells/recipient were resuspended in 100 μL PBS and injected intravenously into NSG. Two weeks after transplant, CLL burden in the peripheral blood of the transplanted recipients (NSGs) was analyzed by flow cytometry and the treatment was initiated. Vehicle control (4% DMSO in corn oil) or 30 mg/kg DAPT was administered daily by i.p. injections for 14 days on a 5 days on–2 days off schedule. Disease burden in the peripheral blood was evaluated by flow cytometry.

RNA library preparation, sequencing, and analysis

RNA was assessed for quality and quantity (RNA 6000 Nano LabChip kit on a 2100 Bioanalyzer; Agilent). RNA libraries were generated using NEBNext Single Cell/Low Input RNA Library Prep Kit for Illumina (New England BioLabs) according to manufacturer's protocol and checked for quality and quantified using the DNA-1000 kit (Agilent) on a 2100 Bioanalyzer. Libraries were sequenced with the Illumina Sequencing SP kit on two lanes to obtain 150-base paired-end (PE) reads. RNA sequencing (RNA-seq) reads were aligned to the mouse reference genome mm10 using STAR (v2.4.0.1; RRID: SCR_004463; ref. 18) and Transcripts Per Kilobase Million (TPM) value was used to measure gene expression. Differentially expressed genes were assessed using DESeq2 (RRID:SCR_000154; ref. 19). Transcription factor and pathway analyses were performed using Enrichr (RRID:SCR_001575) and the TRRUST transcription factor database and the MsigDB hallmark gene sets, respectively.

qPCR

Total RNA was transcribed into cDNA using the SuperscriptII reverse transcription kit (Life Technologies). The expression of mRNAs was analyzed using the TaqMan Gene Expression Assays probes as described in Supplementary Materials and Methods. Target gene expression was normalized to the mean Ct values of the housekeeping gene Gapdh.

DNA isolation and immunoglobulin heavy-chain gene variable region–D-J gene rearrangement analysis

Genomic DNA was isolated using the QIAGEN DNeasy Blood & Tissue Kit (Qiagen). For immunoglobulin heavy-chain gene variable region analysis, DNA from CLL cells was subjected to PCR as previously described (20).

DNA library preparation, HiSeq sequencing, and data analysis

Initial DNA sample quality assessment, DNA library preparation, sequencing, and bioinformatics analysis were conducted at GENEWIZ, Inc. Genomic DNA samples were quantified using Qubit 2.0 Fluorometer (Life Technologies) and DNA integrity was checked with 0.6% agarose gel with 50- to 60-ng sample loaded in each well. SureSelect^{XT} Exome Enrichment System for Illumina Paired-End Multiplexed Sequencing Library and SureSelect Human All Exon V5 bait library were used for target enrichment DNA library

preparation following the manufacturer's recommendations (Agilent) and the standard low-input protocol, which starts with 200 ng. Briefly, the genomic DNA was fragmented by acoustic shearing with a Covaris LE200 Focused Ultra-sonicator instrument. Fragmented DNAs were cleaned up and end-repaired, as well as adenylated at the 3′ends. Adapters were ligated to the DNA fragments, and adapter-ligated DNA fragments were enriched with limited cycle PCR. Adapter-ligated DNA fragments were validated using Agilent TapeStation (Agilent Technologies), and quantified using Qubit 2.0 Fluorometer. Seven hundred and fifty nanograms of adapter-ligated DNA fragments were hybridized with biotinylated RNA baits at 65°C for 24 hours. The hybrid DNAs were captured by streptavidin-coated magnetic beads. After extensive wash, the captured DNAs were amplified and indexed with Illumina indexing primers. Postcaptured DNA libraries were validated using Agilent TapeStation and quantified using Qubit 2.0 Fluorometer and Real-Time PCR (Applied Biosystems). Illumina reagents and kits for DNA library sequencing cluster generation and sequencing were used for enrichment DNA sequencing. Postcaptured DNA libraries were multiplexed in equal molar mass, and pooled DNA libraries were clustered on one lane of a flow cell, using the cBOT from Illumina. After clustering, the flow cell was loaded on the Illumina HiSeq instrument according to manufacturer's instructions. The samples were sequenced using a 2 × 150 PE configuration. Image analysis and base calling was conducted by the HiSeq Control Software (HCS 2.0) on the HiSeq instrument. Whole-exome sequencing raw FASTQ files were aligned to Genome Reference Consortium Mouse Build 38 (mm10) and the resulting BAM files were further processed by marking duplicated reads and recalibrating base qualities. To perform the copy number analysis, read coverage counts were calculated across the exome intervals for all samples. A copy-number variation (CNV) panel of normal (PoN) was created using all of the samples. The tumor read coverage data was normalized using the PoN. All of the analysis was performed following the recommendation of the GATK Best Practices Workflows using GATK4 toolkit (RRID: SCR_001876).

Reduced representation bisulfite sequencing and data analysis

Reduced representation bisulfite sequencing (RRBS) libraries were generated from 50 ng input DNA using the Tecan Ovation RRBS Methyl-Seq System following the manufacturer's recommendation except that we performed scaled-down half reactions from restriction digest through final repair after adapter ligation. Libraries were PCR amplified for 12 cycles. PE 100-base reads were generated on Illumina HiSeq2500 rapid flow cells using custom primers (Tecan) without adding a PhiX spike-in.

Illumina sequencing reads were quality-controlled and adapter clipped using fastQC (RRID:SCR_014583) and cutadapt (21). These reads were aligned to the mouse mm9 reference genome using BSmap (22). In order to determine the methylation state of all CpGs captured and assess the bisulfite conversion rate, we used the mcall module in the MOABS software suite (RRID:SCR_012071) with standard parameter settings (23). Differentially methylated regions (DMR) were called using metilene version 0.2 to 8 (24). DMRs were defined to have an absolute minimum difference in methylation of 0.2 with a maximum distance of 300 nt between CpGs within a DMR and a minimum of 5 CpGs per DMR. Missing values were allowed per group. Adjusted *P* values were calculated using the -c 2 parameters, invoking Benjamini–Hochberg correction (FDR). For heatmap visualization, methylation levels of DMRs were calculated as the mean methylation of all CpGs with a DMR for each sample and plotted using the heatmap function of the R package pheatmap (RRID:SCR_016418). A DMR was associated with a gene if it overlapped or was in the promoter region [(−2500 nt to +500 nt of transcription start site (TSS)] of the respective gene.

Discordant read methylation was calculated from each read based on the fraction of transitions in methylation status (0 or 1) between adjacent CpGs. PE reads overlapping each other were cut in the middle of the overlap to avoid interpretation of the same molecule twice and reads covering less than 3 CpGs were excluded from this analysis. For each read the methylation status of the covered CpGs was determined as unmethylated (converted base) or methylated (unconverted base). Based on this, the number of transitions in methylation status along the read were calculated and normalized to the number of possible transitions.

Data availability

The raw data described in this publication have been deposited in NCBI's Gene Expression Omnibus (GEO) under the accession numbers GSE169245, GSE143711, and GSE122668.

Results

Reduced *DNMT3A* expression is commonly observed in CLL

We reanalyzed transcriptome (RNA-seq) data generated from 107 human CLL samples and $CD19^+$ B cells from 8 HDs (9) to evaluate the expression of *DNMT3A*, *DNMT3B*, and *DNMT1*. We observed robust expression of *DNMT3A* and *DNMT1* in CLLs and HDs, whereas *DNMT3B* was poorly expressed (Supplementary Fig. S1A). Notably, *DNMT3A* expression was highly variable amongst these patients with CLL, and lower *DNMT3A* expression was associated with more aggressive disease with shorter failure-free survival ($P = 0.013$; **Fig. 1A**). We confirmed the high variability in *DNMT3A* expression in CLL in a separate set of 6 HDs and 17 CLLs (Supplementary Fig. S1B). We also validated the correlation between more aggressive disease and low *DNMT3A* expression in another independent cohort consisting of 127 patients with treatment-naïve CLL (Supplementary Fig. S1C; $P = 0.02$). Complementing this analysis, we examined DNMT3A protein expression in 25 CLLs and 6 HDs by Western blot and again found a high degree of expression variability but overall lower expression of DNMT3A in CLLs (Supplementary Fig. S1D–S1F; Supplementary Table S1; $P < 0.001$). Given the known key role of *DNMT3A* across various hematologic malignancies (25–27) and its association with more aggressive CLL that we observed, we sought to evaluate the potential impact for this lesion as a CLL driving event.

B-cell–restricted deletion of *Dnmt3a* leads to generation of CLL

To investigate the role of *DNMT3A* depletion *in vivo*, we generated a B-cell–restricted *Dnmt3a* KO mouse model by intercrossing *Cd19*-Cre and *Dnmt3a*-LoxP mice (**Fig. 1B**), resulting in cohorts of wild-type (*Cd19*-$Cre^{+/-}$, WT), heterozygous KO (*Cd19*-$Cre^{+/-}$ $Dnmt3a^{fl/+}$, referred as $Dnmt3a^{fl/+}$), and homozygous KO (*Cd19*-$Cre^{+/-}Dnmt3a^{fl/fl}$, referred as $Dnmt3a^{fl/fl}$) mice. Successful *Dnmt3a* KO was confirmed by Western blot (**Fig. 1C**), and different groups of mice were monitored for the development of CLL through monthly flow cytometric analysis of peripheral blood for the appearance of $B220^+CD5^+$ cells up to 24 months of age. $Dnmt3a^{fl/fl}$ mice consistently developed CLL between 4 to 8 months of age (median onset of 5.3; $n = 26$) with 100% penetrance (**Fig. 1D**). In contrast, $Dnmt3a^{fl/+}$ mice developed CLL/MBL

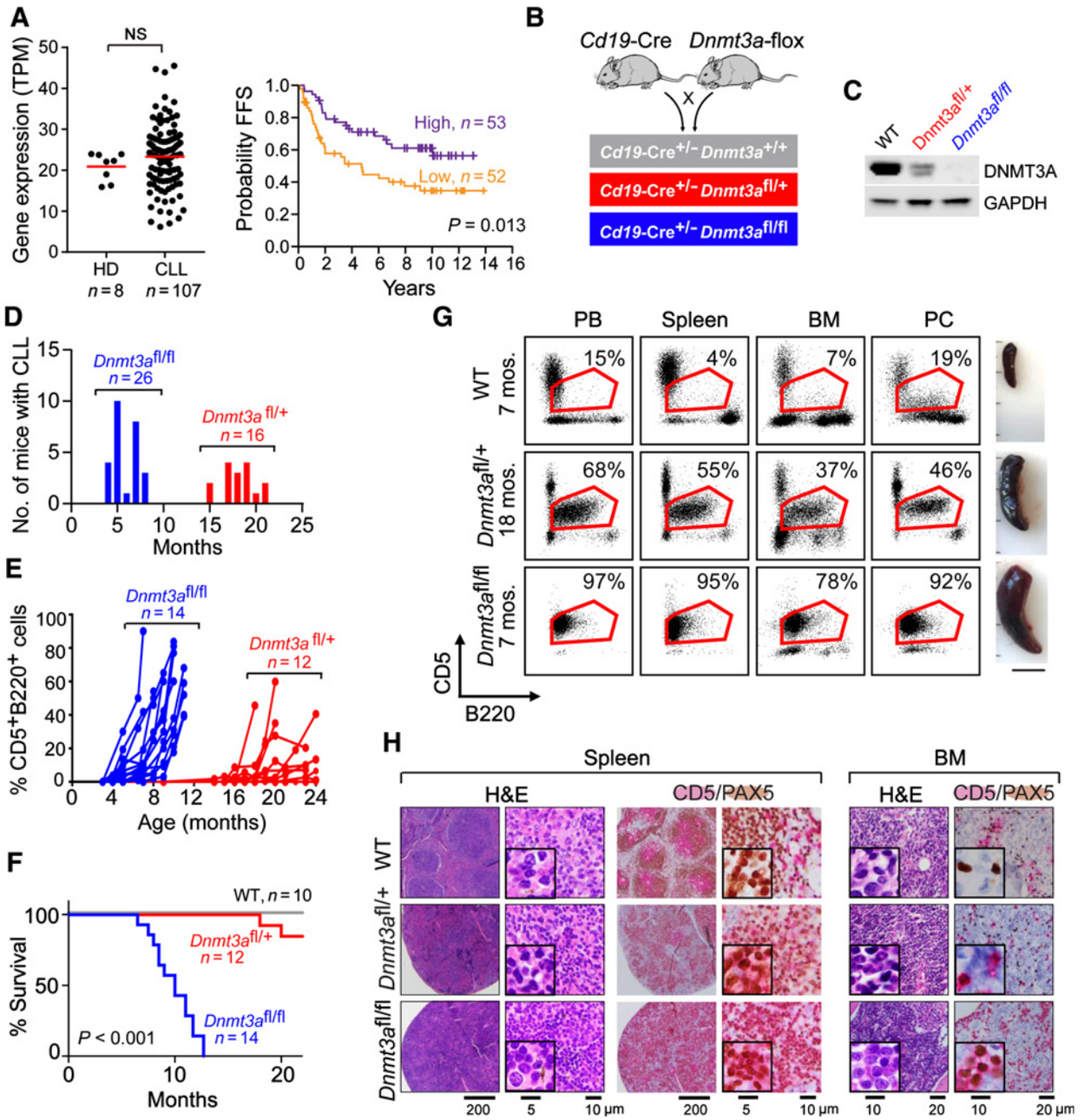

Figure 1.

B-cell–restricted deletion of Dnmt3a leads to CLL. **A,** *DNMT3A* expression in human normal B cells (HD) and CLLs. Failure-free survival (FFS) from the time of sequencing sample to first treatment/progression or death in the *DNMT3A*-high or -low group is shown. Samples were stratified by median *DNMT3A* expression; there were two drop outs. NS, not significant. **B,** Schema of the breeding strategy. **C,** Representative Western blots of DNMT3A expression in splenic B cells across the different genotypes ($n = 3$). **D,** Age of disease onset in *Dnmt3a*$^{fl/+}$ and *Dnmt3a*$^{fl/fl}$ mice. **E,** Detection of B220$^+$CD5$^+$ cells in peripheral blood over time. **F,** Overall survival of WT, *Dnmt3a*$^{fl/+}$, and *Dnmt3a*$^{fl/fl}$ mice over time. **G,** Representative flow cytometry analysis of B220$^+$ CD5$^+$ cells within peripheral blood (PB), spleen, BM, and peritoneal cavity (PC) of WT, *Dnmt3a*$^{fl/+}$, and *Dnmt3a*$^{fl/fl}$ CLL mice, and images of the spleens. Mos., months. **H,** Representative IHC staining of CD5$^+$(red), PAX5$^+$ (brown) of spleen, and BM sections from WT and *Dnmt3a*$^{fl/fl}$ CLL mice. H&E, hematoxylin and eosin.

between 15 to 21 months of age (median of 18.5; $n = 16$) with 89% penetrance, while none of the *Cd19*-Cre$^{+/-}$ control mice developed CLL. No malignancies other than CLL were observed in *Dnmt3a* KO mice over this time period, as confirmed by IHC. A subset of mice was further monitored for disease progression and survival, showing that CLL progressed rapidly in the *Dnmt3a*$^{fl/fl}$ mice ($n = 14$), resulting in poorer survival than the *Dnmt3a*$^{fl/+}$ mice ($n = 12$; **Fig. 1E** and **F**).

Mice with CLL consistently displayed enlarged spleens, with infiltration of CLL cells in the peripheral blood, spleen, BM, and peritoneal

cavity of affected mice (**Fig. 1G**). The presence of CLL cells in the BM and spleen was confirmed by colocalization of CD5 (red) and PAX5 (brown) expression within the tissue sections (**Fig. 1H**). We confirmed that the CLL cells were clonal based on Igκ expression and immunoglobulin heavy-chain gene variable region (IGHV) mutational status (20), which was found to be unmutated (i.e., 100% homology with germline) in all 5 samples tested (Supplementary Table S2). We further confirmed the transplantability of the CLL cells. Following intravenous injection of CLL cells into immunodeficient mice (NSG; $n = 5$), we consistently detected CLL cells in the peripheral blood of recipient mice 4 weeks following transplant. In each instance, upon euthanasia at 6 weeks following injection, these CLL cells were also detected in the spleen, BM, and peritoneal cavity by flow cytometry (Supplementary Fig. S1G). Altogether, we demonstrate that CD19-restricted deletion of *Dnmt3a* reliably results in CLL, confirming this lesion as a CLL driving event.

B-cell–restricted loss of *Dnmt3a* expression alters B-cell development in preleukemic animals

We examined the impact of *Dnmt3a* depletion on normal B-cell development in 2- to 3-month old preleukemic mice using previously established flow cytometry conditions (Supplementary Fig. S2A and S2B; refs. 3, 4). Splenocytes from *Dnmt3a* KO mice were reduced in a proportion of marginal zone cells (MZ; $B220^+;CD23^-;CD21^+$; $P < 0.001$, Student *t* test) and increased in a proportion of follicular B cells (FO; $B220^+;CD23^+;CD21^-$; $P < 0.02$, Student *t* test) compared with WT mice (**Fig. 2A**). In contrast, no proportion differences in BM B-cell subpopulations were observed (Supplementary Fig. S2C). Of note, splenic B cells from *Dnmt3a* KO mice exhibited no alteration in BCR signaling activity (Supplementary Fig. S2D) or immune response to sheep red blood cells (Supplementary Fig. S2E) compared with WT B cells, which differs from our previously reported CLL mouse models (3, 4).

We detected a substantially increased proportion of $CD11b^+$ B1a cells ($CD19^+;CD43^+;CD5^+;CD11b^+$) in the peritoneal cavity of $Dnmt3a^{fl/fl}$ mice (**Fig. 2B**), suggesting B1a cells as the cell of origin of CLL in this model system. Testing this hypothesis, we transplanted marrow hematopoietic stem cells (LSK cells; $n = 5$) or B1a cells ($n = 5$) isolated from $Dnmt3a^{fl/fl}$ mice into irradiated $CD45.1^+$ recipient mice. While no recipient mice transplanted with LSKs developed CLL up to 12 months following transplantation, clonal $CD45.2^+B220^+CD5^+Igk^+$ CLL cells were detectable in peripheral blood of recipient mice transplanted with B1a cells starting 10 weeks after transplantation (**Fig. 2C**). IHC staining of splenic and BM tissue sections confirmed the presence of CD5 and PAX5 double-positive CLL cells among the engrafted cells (**Fig. 2D**). Infiltration of CD45.2 CLL cells was evident in the peripheral blood, spleen, BM, and peritoneal cavity of affected mice (Supplementary Fig. S2F and S2G). Consistent with the parental model, CLL cells exhibited no obvious alteration in BCR signaling activity (Supplementary Fig. S2H). Together, these data support the notion that CLL cells in this model arise from the B1a population.

To determine the mechanism of $Dnmt3a^{fl/fl}$ B1a cell expansion, we analyzed cell division of B1a cells from WT or $Dnmt3a^{fl/fl}$ animals using CFSE staining. Peritoneal cells were isolated, labeled with CFSE, and injected intraperitoneally into irradiated immunodeficient recipients (NSG; $n = 5$). Cell division was assessed by measuring the corresponding decrease in cell fluorescence via flow cytometry. Since no difference ($P = 0.72$) in cellular proliferation between the 2 groups was observed (**Fig. 2E**), we asked whether $Dnmt3a^{fl/fl}$ B1a expansion was caused by reduced cell death. Indeed, both splenic $CD19^+$ B cells and peritoneal B1a cells from $Dnmt3a^{fl/fl}$ mice showed reduced apoptotic priming, induced by BH3 peptides (i.e., BIM and PUMA), compared with WT cells (**Fig. 2F**). *Dnmt3a* depletion thus appears to affect B1a expansion through a reduction in cell death, rather than increased proliferation.

Dnmt3a deletion alters the methylomes and transcriptomes of preleukemic B1a cells

Given the known role of *Dnmt3a* as a *de novo* methyltransferase, we evaluated the impact of *Dnmt3a* depletion on global DNA methylation of preleukemic B1a cells (i.e., absence of circulating CLL cells at the time of analysis) and of B2 cells (as a comparator population), using RRBS. Although no difference in the average CGI methylation levels was observed between $Dnmt3a^{fl/fl}$ versus WT B cells ($n = 3$ per group; **Fig. 3A**), increased local methylation disorder [measured by percent discordant reads (PDR)] was observed in CGI shelves and background regions (i.e., CpG sites that are not in CpG islands, shores, or shelves) in $Dnmt3a^{fl/fl}$ B1a cells compared with WT B1a cells (**Fig. 3B**). We identified a set of DMRs (difference > 0.2; Supplementary Table S3), mostly hypomethylated, in $Dnmt3a^{fl/fl}$ versus WT B1a cells (**Fig. 3C** and **D**). As representative examples, hypomethylated DMRs in the promoter regions of the *Cxcr7*, *Wnt10b*, and *Hes5* genes are shown in **Fig. 3E**. In contrast, only minor changes in methylation were observed in $Dnmt3a^{fl/fl}$ B2 cells. Notably, complete depletion of *Dnmt3a* was confirmed by RNA-seq in both $Dnmt3a^{fl/fl}$ B1a and B2 cells (Supplementary Fig. S3A), suggesting that the methylation differences between the cell types could not be attributed to incomplete KO of *Dnmt3a* in B2 cells. As *DNMTs* might have overlapping functions to regulate DNA methylation, we quantified the expression of *Dnmt3a*, *Dnmt3b*, and *Dnmt1* by real-time PCR in these cells. Our results revealed higher levels of *Dnmt3b* ($P = 0.005$) in B2 cells compared with B1a cells (Supplementary Fig. S3B), suggesting that *Dnmt3b* might functionally compensate for the loss of *Dnmt3a* in $Dnmt3a^{fl/fl}$ B2 cells. We further confirmed that *Dnmt3b1*, the active isoform of *Dnmt3b* gene, was stably expressed in $Dnmt3a^{fl/fl}$ B2 cells (Supplementary Fig. S3C). Pathway analysis revealed that genes associated with those DMRs were highly enriched in *Notch*, TNFα, TGF-β, and IL2/STAT5 signaling, and apoptosis (Supplementary Table S4).

Given the prominent hypomethylation changes observed in *Dnmt3a* depleted B1a cells, we investigated whether these would lead to altered gene transcript expression. Indeed, principal component analysis (PCA) of bulk transcriptomes generated from $Dnmt3a^{fl/fl}$ and WT B1a, and B2 cells ($n = 3$ per group) revealed clear differences between $Dnmt3a^{fl/fl}$ and WT B1a cells, but not between $Dnmt3a^{fl/fl}$ and WT B2 cells, in line with the methylation changes (**Fig. 3F**). However, in *Dnmt3a*-depleted B1a cells, hypomethylation events were not necessarily associated with upregulation of gene expression (Supplementary Fig. S3D), suggesting that the methylation status per se was insufficient to determine gene expression, in line with prior findings (28). Nevertheless, we detected 460 downregulated and 168 upregulated genes in the $Dnmt3a^{fl/fl}$ B1a cells compared with WT B1a cells [**Fig. 3G**, left; FDR < 0.05, fold change (FC) > 2; Supplementary Table S5], while the changes in B2 cells were negligible (**Fig. 3G**, right). Differentially expressed genes in $Dnmt3a^{fl/fl}$ B1a were highly enriched for several oncogenic signaling pathways, including *Notch*, TNFα, JAK/STAT3, and *Wnt*-β catenin signaling (**Fig. 3H**; Supplementary Table S6).

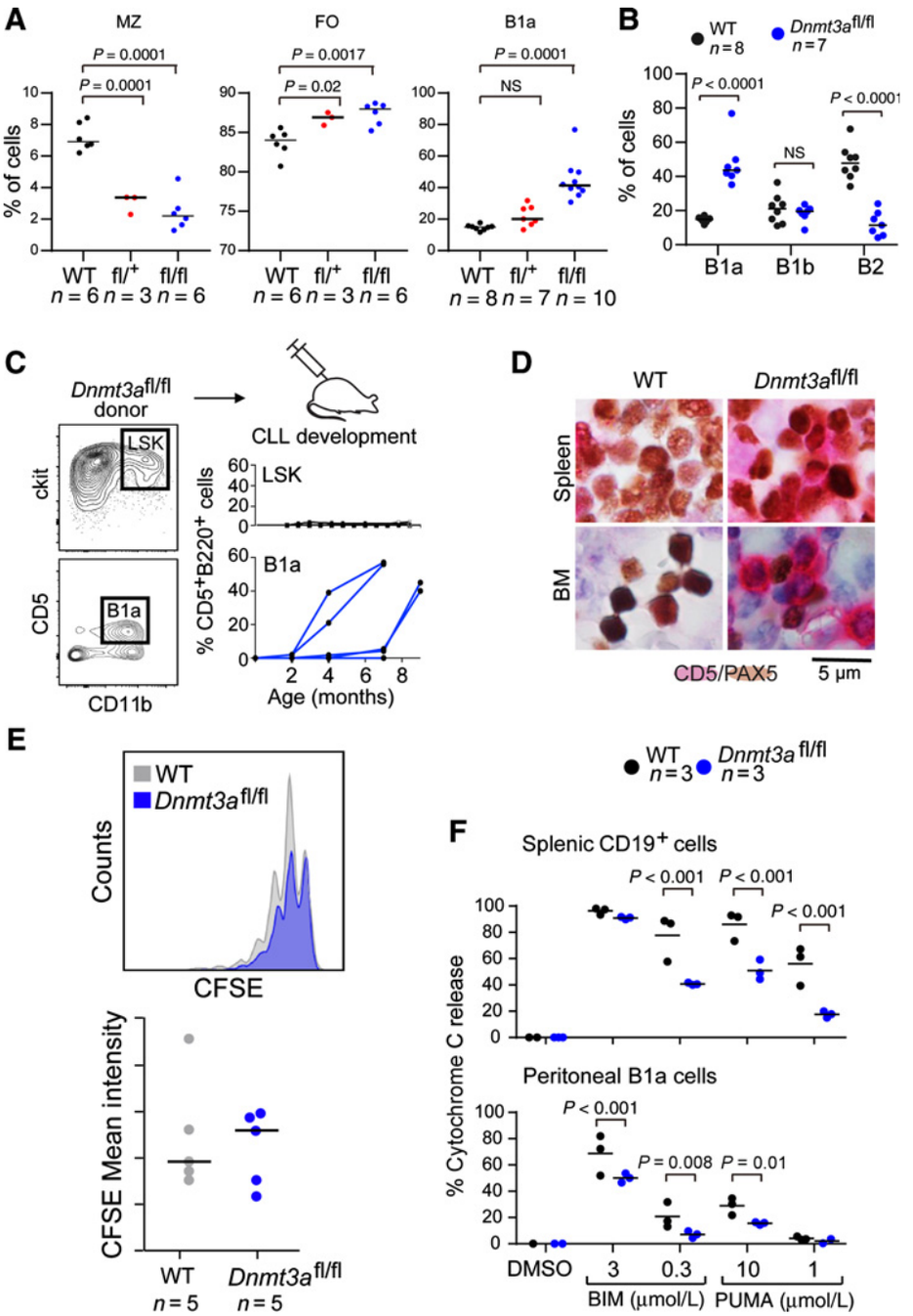

Figure 2.

B1a cell expansion in the peritoneal cavity of *Dnmt3a*$^{fl/fl}$ mice results in CLL development. **A,** Analysis of the percentage of MZ B cells and FO B cells from the total splenocyte suspension and the percentage of B1a from peritoneal B cells of WT and *Dnmt3a*$^{fl/fl}$ mice. Data were compared using one-way ANOVA followed by Dunnett multiple comparison test. **B,** Proportions of BM B-cell subpopulations. NS, not significant. **C,** Transfer of Lin$^-$;Scal$^+$;c-kit$^+$ (LSK) or B1a cells from *Dnmt3a*$^{fl/fl}$ or WT donor mice to CD45.1 recipient mice, and flow cytometry analysis of B220$^+$ CD5$^+$ cells within peripheral blood over time ($n = 5$). **D,** Representative IHC staining of CD5$^+$ (red) and PAX5$^+$ (brown) of spleen and BM sections from CD45.1 recipient mice following transfer of B1a cells from WT and *Dnmt3a*$^{fl/fl}$ CLL mice. **E,** B1a cells were isolated from WT and *Dnmt3a*$^{fl/fl}$ mice, stained with CSFE, and injected intraperitoneally into CD45.1 recipient mice. B1a cells were analyzed for CFSE intensity by flow cytometry 11 days after injection. **F,** BH3 profiles of peritoneal B1a cells and splenic CD19$^+$ cells.

Changes in methylome and transcriptome associated with CLL development

Upon investigating the methylomes of the CLL cells arising in *Dnmt3a*$^{fl/fl}$ animals compared with WT and *Dnmt3a*$^{fl/fl}$ B1a cells, we observed a marked increase in CGI methylation rate in CLL cells (**Fig. 4A**). This was accompanied by increased PDR levels in background regions and CpG shelves, and decreased PDR levels in CpG islands (**Fig. 4B**). Notably, we identified multiple DMRs in CLL cells compared with either WT or *Dnmt3a*$^{fl/fl}$ B1a cells (difference > 0.2; **Fig. 4C–E**; Supplementary Tables S7 and S8), a large fraction of which were hypermethylated. In the promoter regions of the CLL cells, we identified 1,514 hypermethylated and 247 hypomethylated DMRs compared with WT B1a cells, and 1,574 hypermethylated and 103 hypomethylated DMRs compared with *Dnmt3a*$^{fl/fl}$ B1a cells. In gene body regions, we identified 855 hypermethylated and 1,088 hypomethylated DMRs compared with WT B1a cells, and 892 hypermethylated and 503 hypomethylated DMRs compared with *Dnmt3a*$^{fl/fl}$ B1a cells (examples of the differentially methylated DMRs in the promoters shown in **Fig. 4F**). Of the 466 hypomethylated DMRs observed in the preleukemia *Dnmt3a*$^{fl/fl}$

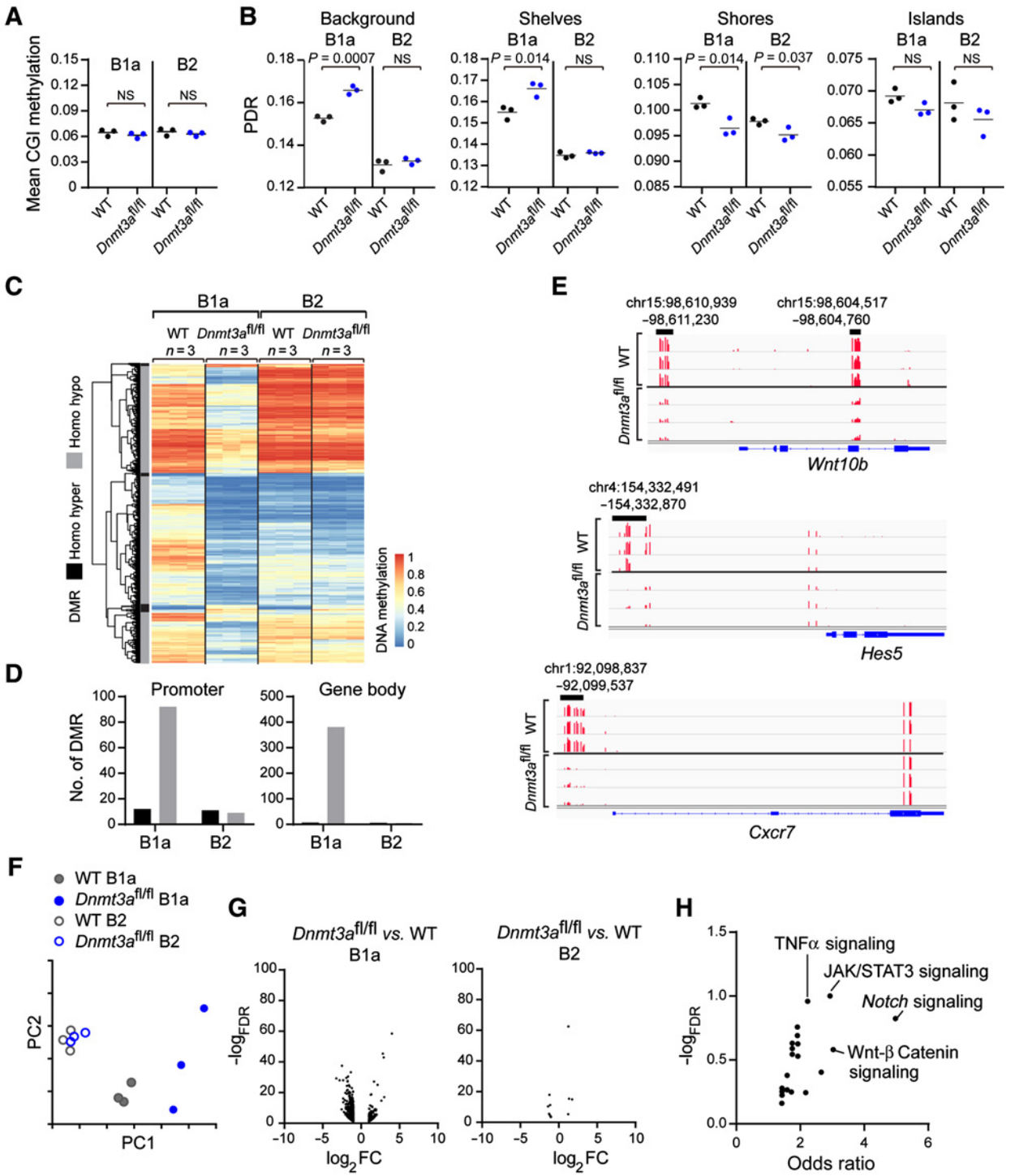

Figure 3.

Changes in methylome and transcriptome associated with *Dnmt3a* depletion in preleukemic B cells. **A,** Mean CGI methylation in WT ($n = 3$) and *Dnmt3a*$^{fl/fl}$ ($n = 3$) B1a or B2 cells. NS, not significant. **B,** PDR associated with different DNA regions in different cells. CGIs were downloaded from the UCSC Genome Browser (defined as regions > 500 bp, > 55% GC, and expected/observed CpG ratio of >0.65), CGI shores ±2Kb from islands, and CpG shelves ±2Kb from CGI shores. All the other regions were defined as background ($n = 3$). **C,** Heatmap of DMRs between WT and *Dnmt3a*$^{fl/fl}$ B1a or B2 cells ($n = 3$ each). **D,** Number of DMRs between *Dnmt3a*$^{fl/fl}$ and WT B1a or B2 cells associated with promoter regions or gene body. **E,** Examples of DMRs in *Dnmt3a*$^{fl/fl}$ B1a cells versus WT B1a cells. **F,** PCA of transcriptome data of WT and *Dnmt3a*$^{fl/fl}$ B1a or B2 cells. **G,** Volcano plots of differentially expressed genes between *Dnmt3a*$^{fl/fl}$ versus WT B1a or B2 cells. **H,** Signaling pathways enriched for differentially expressed genes in *Dnmt3a*$^{fl/fl}$ B1a cells versus WT B1a cells.

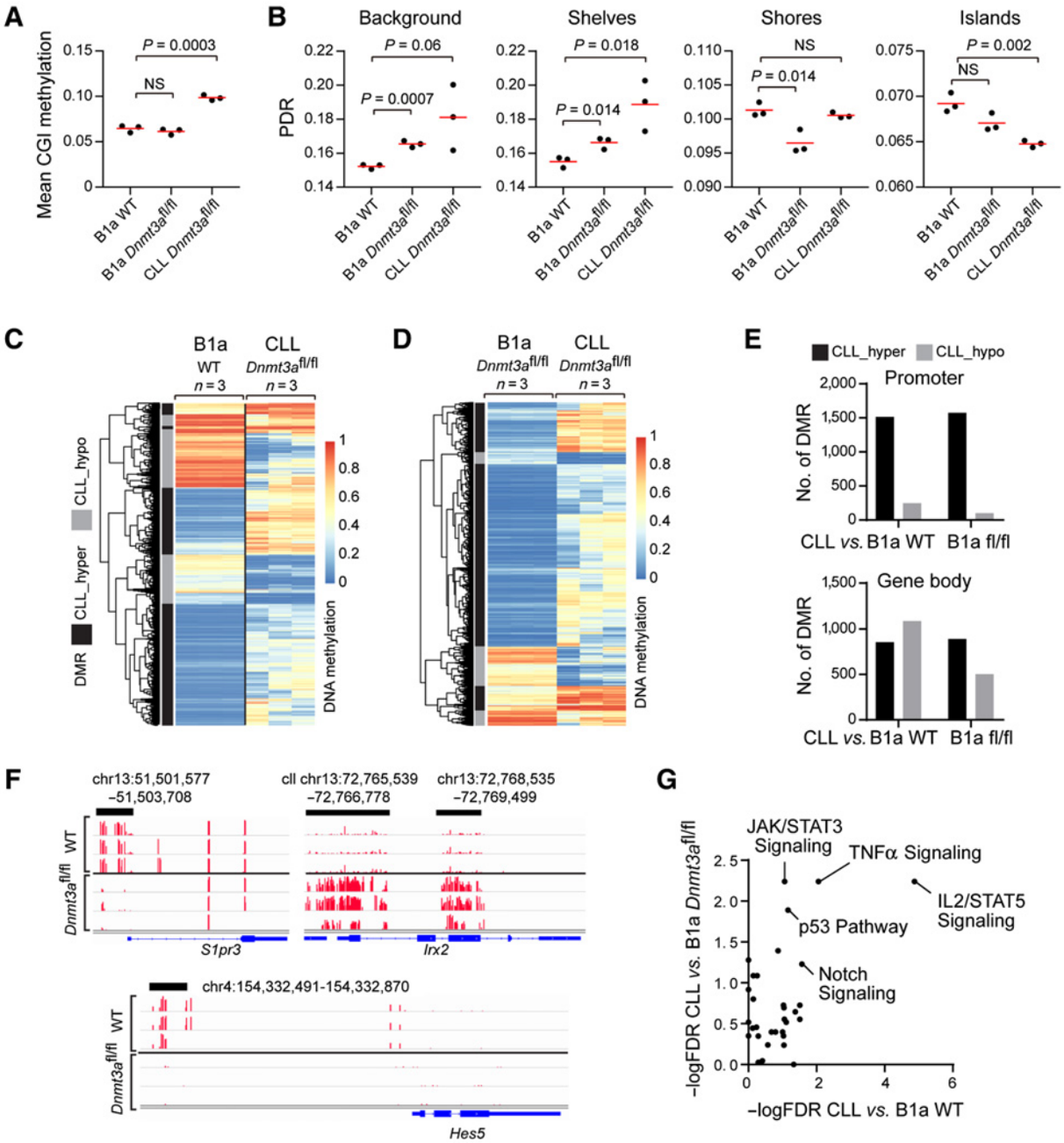

Figure 4.

Changes in methylome and transcriptome associated with *Dnmt3a*-depleted CLL cells. **A,** Mean CGI methylation in WT and *Dnmt3a*$^{fl/fl}$ B1a or CLL cells ($n = 3$). NS, not significant. **B,** PDR associated with different DNA regions in different cells. CGIs were downloaded from the UCSC Genome Browser (defined as regions >500 bp, >55% GC, and expected/observed CpG ratio of >0.65), CGI shores ±2 Kb from islands, and CpG shelves ±2 Kb from CGI shores ($n = 3$). **C,** Heatmap of DMRs between *Dnmt3a*$^{fl/fl}$ CLL cells and WT B1a. **D,** Heatmap of DMRs between *Dnmt3a*$^{fl/fl}$ B1a and *Dnmt3a*$^{fl/fl}$ CLL cells ($n = 3$ each). **E,** Number of DMRs in *Dnmt3a*$^{fl/fl}$ CLLs versus *Dnmt3a*$^{fl/fl}$ or WT B1a cells associated with promoter regions or gene body. **F,** Examples of DMRs in *Dnmt3a*$^{fl/fl}$ CLL cells versus WT B1a cells. **G,** Signaling pathways enriched for differentially expressed genes between *Dnmt3a*$^{fl/fl}$ CLL cells versus WT B1a cells, as well as between *Dnmt3a*$^{fl/fl}$ CLL cells versus *Dnmt3a*$^{fl/fl}$ B1a cells.

B1a cells (Supplementary Table S3), only 45 remained hypomethylated in *Dnmt3a*$^{fl/fl}$ CLL cells compared with WT B1a (including *Hes5*), and the others remained unchanged ($n = 383$) or even hypermethylated ($n = 38$), suggesting a dramatic reprogramming of the methylation profile associated with progression to CLL. Genes with promoter and/or gene body DMRs in CLL compared with WT B1a cells were highly enriched for several oncogenic signaling pathways including *Notch* and

Hedgehog signaling, epithelial–mesenchymal transition, and *Wnt* signaling (Supplementary Table S9).

RNA-seq analysis of *Dnmt3a*$^{fl/+}$ and *Dnmt3a*$^{fl/fl}$ CLLs ($n = 3$ each) revealed that expression changes in *Dnmt3a*$^{fl/+}$ and *Dnmt3a*$^{fl/fl}$ CLLs compared with WT B1a cells were highly concordant (Supplementary Fig. S3E; R = 0.72, $P < 0.0001$), suggesting a consistent transcriptional reprogramming during CLL development. We thus combined the 2 groups to identify commonly altered genes in CLL cells. We identified more upregulated ($n = 2801$) than downregulated ($n = 1{,}244$) genes in CLL cells compared with WT B1a cells (FDR < 0.05, FC > 2; Supplementary Table S10). Moreover, we identified 3,030 upregulated and 1,652 downregulated genes in CLL versus *Dnmt3a*$^{fl/fl}$ B1a cells (Supplementary Table S11). To determine the signaling pathways affected in CLL cells, we performed an unbiased pathway enrichment analysis of these differentially expressed genes using MSigDB hallmark gene sets. This allowed us to identify several pathways that were commonly enriched in both comparisons; again, we observed enrichment of *Notch* signaling genes (**Fig. 4G**; Supplementary Table S12), pointing to its putative important role in CLL development.

Compared with methylome data of human CLLs (11), we identified 20 hypermethylated genes and 210 hypomethylated genes that are shared between human and mouse CLLs. The 444 DMRs of these genes in human CLLs are shown in Supplementary Table S13. These genes were highly enriched for TGF-β signaling, UV response, and mitotic spindle (all FDR < 0.005), supporting a role of DNA damage repair pathway in CLL development. To determine the gene signatures associated with poor *DNMT3A* expression in human CLL, we reanalyzed transcriptome profiles of 8 samples with the lowest *DNMT3A* expression in the cohort (**Fig. 1A**). Compared with normal B cells ($n = 8$), altogether there were 715 upregulated and 428 downregulated genes in these CLLs (FC > 2, FDR < 0.05). Of these genes, we identified 104 upregulated and 18 downregulated genes that overlapped with the *Dnmt3a* mouse CLL model (Supplementary Table S14). Pathway analysis revealed that these genes were highly enriched for apical junction, IL2/STAT5 signaling and complement (all FDR < 0.05).

Hyperactivation of *Notch* and *Myc* signaling in *Dnmt3a*$^{fl/fl}$ CLL

Closer inspection of the role of the *Notch* signaling pathway in the *Dnmt3a*-depleted CLL models revealed a general upregulation of *Notch* signaling genes in CLL cells compared with either WT or *Dnmt3a*$^{fl/fl}$ B1a cells (**Fig. 5A**). To investigate whether upregulation of *Notch* signaling genes was associated with abnormal activation of the signaling pathway, we examined expression changes of known *Notch* targets in these CLL cells (29). As a comparison, we also examined *Notch* target expression in three other CLL genetically engineered mouse models, namely those driven by *MDR*, *Ikzf3*, or *Sf3b1-Atm* lesions (**Fig. 5B**; refs. 3, 4, 15). The distinct features of these mouse models are summarized in Supplementary Fig. S3F. Indeed, we observed high variability of *Notch* target expression across the different CLL models, with selective upregulation of Notch targets exclusively observed in the *Dnmt3a*-depleted CLL model but not in others (**Fig. 5C**). The results remained robust even after we separated *Dnmt3a*$^{fl/+}$ CLLs from *Dnmt3a*$^{fl/fl}$ CLLs, supporting a unique role of *Notch* activation in this model (Supplementary Fig. S3G). We were able to validate upregulation of several well established *Notch* targets (i.e., *Hes5*, *Dtx1*, and *St3gal6*) in CLL cells versus normal B cells (**Fig. 5D**).

To examine the therapeutic vulnerabilities of the diverse genetic CLL models to various drugs, we exposed CLL cells to the BCL2 inhibitor ABT-199 (venetoclax), BTK inhibitor ibrutinib, the *Notch* signaling inhibitor DAPT, the *Wnt* signaling inhibitor LGK-974, and DMSO. The optimal working concentration of different drugs had been determined by treating tumor cells with multiple doses (Supplementary Fig. S4A). CLL cells from the four distinct CLL models were treated with two concentrations of each drug for 24 hours, and percent survival was calculated as the ratio between the cellular viability following test drug exposure and DMSO. *Dnmt3a*-depleted CLLs were more sensitive to ABT than the other CLLs, consistent with the BH3 results suggesting that *Dnmt3a*-depleted CLLs were more dependent on BCL2 for survival (Supplementary Fig. S4B). Moreover, *Dnmt3a*-depleted CLL cells were highly sensitive to *Notch* inhibition by DAPT (**Fig. 5E**; Supplementary Fig. S4C), supporting hyperactivation of *Notch* signaling in these CLL cells and high dependency on this pathway for survival. *In vivo*, NSG mice transplanted with *Dnmt3a*$^{fl/fl}$ CLLs and subsequently treated with DAPT (30 mg/kg; $n = 5$) or DMSO ($n = 5$) for 14 days likewise showed highly sensitivity to treatment with *Notch* inhibition (**Fig. 5F**; $P = 0.008$).

To determine if *Dnmt3a*$^{fl/fl}$ CLLs had a distinct genetic profile, we performed whole-genome sequencing of the CLL cells. Notably, our analysis revealed amplification of chromosome 15 in these CLL cells (**Fig. 5G**), consistent with our other genetically engineered CLL models (3, 4), and thereby suggesting a common oncogenic mechanism contributing to CLL generation. A putative oncogenic driver localized in chromosome 15 is *Myc*, a direct downstream target activated by *Notch* signaling. Consistent with *Myc* copy number gain, IHC staining of spleen sections also revealed strong upregulation of MYC protein expression in *Dnmt3a*$^{fl/fl}$ CLLs compared with WT B cells (**Fig. 5H**). In line with this notion, we observed that a large fraction of known *Myc* targets in B cells (30) were preferentially upregulated in CLL cells versus normal B cells (**Fig. 5I**). In contrast, very few somatic mutations (26 and 32, respectively) were identified in these CLL samples (Supplementary Table S15).

To determine if the aforementioned insights identified in our mouse model were reflected in human CLL, we evaluated the relationship between baseline expression of *DNMT3A* and sensitivity to *Notch* inhibition in primary untreated CLL samples (Supplementary Table S16). Nine samples with differing levels of *DNMT3A* were exposed to 50 μmol/L DAPT, 1 nmol/L ABT-100, or 1 μmol/L ibrutinib overnight followed by CellTiter-Glo assessment of cellular viability (31–33). Primary CLLs with lower expression of *DNMT3A* were more sensitive to DAPT, but not to the other two drugs, supporting a specific dependence on *Notch* signaling for survival (**Fig. 5J**). Moreover, activation of *Notch* signaling through coculturing with *Notch* ligand–expressing OP9 stroma could sensitize *DNMT3A*-high CLLs ($n = 5$) to DAPT (Supplementary Fig. S4D), again supporting a direct link between *Notch* activity and the observed drug response.

Discussion

DNMT3A is essential for *de novo* DNA methylation and its inactivation in embryos results in lethally of mice at 4 weeks of age (34). In blood malignancies, dysregulation of Dnmt3a, whether by mutation or altered expression, is increasingly appreciated to be crucial to the pathogenesis of both myeloid and lymphoid malignancies. Dnmt3a is essential for hematopoietic stem cell differentiation, and hematopoietic lineage skewing was observed in its absence (35, 36). Previous murine model studies have only occasionally identified CLL resulting from disruption of *Dnmt3a* expression, while developing aggressive myeloid or lymphoid neoplasms with early (<12 month) onset

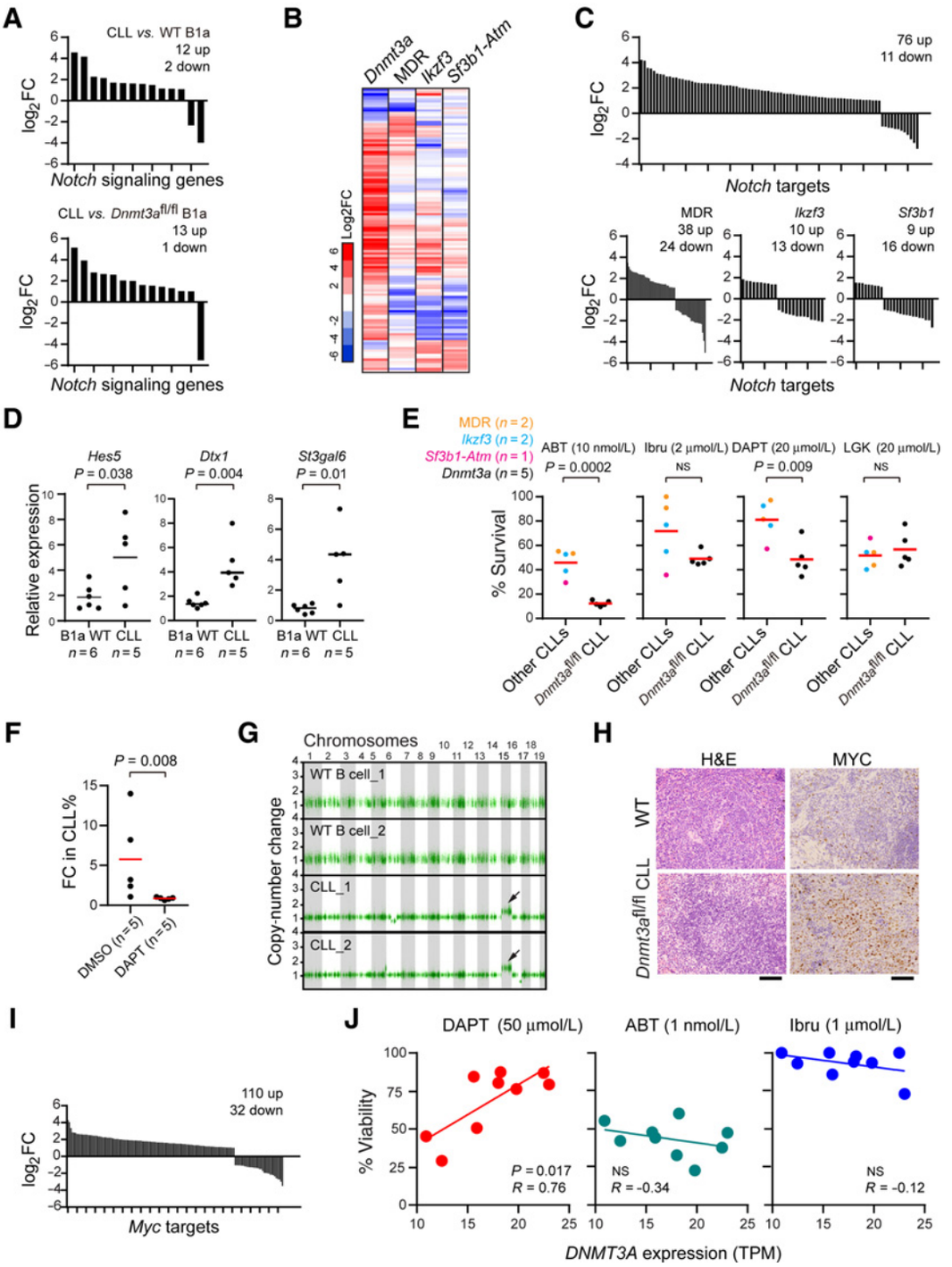

Figure 5.

Activation of *Notch/Myc* signaling in *Dnmt3a*$^{fl/fl}$ CLLs. **A,** Changes in expression of significantly altered *Notch* signaling genes in *Dnmt3a*$^{fl/fl}$ CLLs versus WT B1a cells. **B,** Heatmap of change in expression of *Notch* signaling genes in different mouse models. **C,** Changes in significantly altered *Notch* target genes in different CLL mouse models. **D,** qPCR analysis of expression of well-known *Notch* target genes in different cells. **E,** Sensitivity of different CLL cells with various driver mutations to different drugs, including the BCL2 inhibitor ABT-199 (venetoclax, ABT), the BTK inhibitor ibrutinib (Ibru), the *Notch* signaling inhibitor DAPT, and the *Wnt* signaling inhibitor LGK-974 (LGK). **F,** FC (day 14 vs. day 0) of the percentage of circulating CLL cells of transplanted mice treated with DMSO or 30 mg/kg DAPT. **G,** Copy-number analysis of WT B cells or *Dnmt3a*$^{fl/fl}$ CLL ($n = 2$). Arrows, amplification of Chr 15. **H,** IHC analysis of *Myc* in spleen sections of *Dnmt3a*$^{fl/fl}$ CLLs versus WT B1a cells. H&E, hematoxylin and eosin. **I,** Change in expression of *Myc* targets in *Dnmt3a*$^{fl/fl}$ CLLs versus WT B1a cells. **J,** The correlation between DNMT3A expression and response to different drugs in human primary CLLs ($n = 9$) *in vivo*, measured by CellTiter-Glo. NS, not significant. Scale bar, 50 μm.

(Supplementary Table S17). Conditional KO of *Dnmt3a* in *Mx1*-Cre; *Dnmt3a*$^{fl/fl}$ mice by pIpC treatment, followed by transplantation of whole BM cells predominantly resulted in myeloid neoplasms, including myelodysplastic syndromes (MDS; 76%), acute myelogenous leukemia (AML; 8%), and MDS/myeloproliferative neoplasms (MPN; 16%; ref. 37). Interestingly, deletion of Dnmt3a together with expression of mutant c-Kit lead to the development of B-ALL in 25% of the mice, suggesting cooperation between the two mutations is necessary for acute B-cell lymphomagenesis (37). In parallel studies, irradiated mice transplanted with *Mx1*-Cre;*Dnmt3a*$^{fl/fl}$ HSCs develop wide spectrum of blood malignancies, including T-cell and B-cell acute lymphocytic leukemia, myelodysplastic syndrome, acute myeloid leukemia, and primary myelofibrosis (16, 38, 39). In contrast, when homozygous *Dnmt3a* KO in HSCs through the EmSR-tTA;Teto-Cre system, peripheral T-cell lymphomas (PTCL) and CLL were observed, whereas heterozygous deletion of *Dnmt3a* resulted in MBL/CLL (65% of the cases) and myeloproliferative disease (MPD, 15%; refs. 40–42). In another study, deletion of Dnmt3a specifically in B cells resulted in expansion of B1a cells and development of monoclonal leukemia (43). Finally, deletion of *Dnmt3a* using the Vav-Cre; *Dnmt3a*$^{fl/fl}$ model resulted in MDS (53%), AML (7%), MPN (7%), and mixed phenotype acute leukemia (13%; ref. 44). The heterogeneity of disease phenotypes observed in these studies may be explained by the distinct conditional strategies, as Mx1-cre and Vav1-cre are known to impact transgene expression also in non-HSC populations, including endothelial and BM mesenchymal cells (45). Overall, all these studies support the role of Dnmt3a as a tumor suppressor across cell lineages.

In this study, by restricting *Dnmt3a* loss to B cells through intercrossing with CD19-Cre mice, we detected only the generation of CLL (without occurrence of myeloid disease or PTCL). Alterations in methylation produced by lack of *DNMT3A* present within the distinct cellular context and transcriptional regulatory milieu of B1a cells consistently led to disease. Notably, we identified that *DNMT3A* depletion resulted in the activation of the key CLL-associated pathway of *Notch* signaling as well as *Myc* overexpression. Thus, distinct from other existing genetically engineered mouse models of CLL, which prominently feature dysregulation of BCR signaling, this *DNMT3A*-depleted model most critically dysregulates *Notch*. As NOTCH mutations and altered expression have been highly linked to CLL generation, our results provide a novel mechanism linking epigenetic alterations in CLL to *NOTCH* dysregulation.

Our analysis of the changes in the methylation profiles of our heterozygous and homozygous *Dnmt3a* KO mouse models and the mechanism of *Notch* activation within these models provided us with insight into the process by which *Dnmt3a* depletion exerts its pro-oncogenic activity. To determine the influence of *Dnmt3a* depletion on methylation we performed RRBS analysis. The principle of RRBS is to focus coverage on CpG dense regions of the genome, but not the whole genome, in order to reduce sequencing requirements and cost. Using RRBS, about 50% of covered CpGs are located in CpG islands (CGI) and the remaining CpGs span other CpG dense regions including gene bodies and repeats. Of note, CGIs are often located close to gene promoters, and methylation of CGIs is one of the major mechanisms of gene-expression regulation (46). We observed two levels of change in the DNA methylation profiles within our models. In the preleukemic setting, we found that loss of *Dnmt3a* induced limited but significant hypomethylation whose impact was reduced apoptotic priming and facilitated accumulation of B1a cells. Following CLL transformation, we observed the CLL cells to become hypermethylated. This process was seemingly independent of *Dnmt3a* function as this is also observed in other CLL mouse models with WT *Dnmt3a*, suggesting that the hypermethylation is a response to, rather than a cause of, CLL progression, in line with prior findings (28). In combination with Dnmt3a-associated methylation changes, these result in transcriptional dysregulation of several oncogenic pathways that are important for CLL development, particularly *Notch* signaling.

Altogether, we identified an association between low *DNMT3A* expression and poor failure-free survival in human datasets, and have confirmed a causal role of *Dnmt3a* depletion in CLL generation in mice. Our results support the interaction between *Dnmt3a*-dependent methylation change and activation of *Notch and Myc* signaling as a mechanism by which *Dnmt3a* depletion induces CLL. Moreover, the *Dnmt3a* models provide a unique opportunity for the study of non-mutational *Notch* activation, and a useful platform for the study of *Notch*-signaling targeted therapeutics.

Authors' Disclosures

C.J. Wu is an equity holder of BioNtech, Inc. and C.J. Wu and D.S. Neuberg receive research funding from Pharmacyclics. D.S. Neuberg has been a consultant for H3 Biomedicine and received research funding from Celgene. A. Letai serves as an equity holding SAB member for Zentalis Pharmaceuticals, Flash Therapeutics, and Dialectic Therapeutics. His laboratory receives research support from Novartis. T.J. Kipps has received research funding and/or has served as an advisor to Ascerta/AstraZeneca, Celgene, Genentech/Roche, Gilead, Janssen, Loxo Oncology, Octernal Therapeutics, Pharmacyclics/AbbVie, TG Therapeutics, VelosBio, and Verastem. Cirmtuzumab was developed by T.J. Kipps and licensed by the University of California to Oncternal Therapeutics, Inc., which has provided stock/options to the university and T.J. Kipps. C. Sun received research funding from Genmab. J.R. Brown has served as a consultant for Abbvie, Acerta/Astra-Zeneca, Beigene, Bristol-Myers Squibb/Juno/Celgene, Catapult, Eli Lilly, Genentech/Roche, Janssen, MEI Pharma, Morphosys AG, Nextcea, Novartis, Pfizer, Rigel; received research funding from Gilead, Loxo/Lilly, SecuraBio, Sun, TG Therapeutics; and served on the data safety monitoring committee for Invectys. No disclosures were reported by the other authors.

Authors' Contributions

A. Biran: Conceptualization, writing–review and editing, formal analysis, data curation. **S. Yin:** Conceptualization, data curation, formal analysis, writing–review and editing. **H. Kretzmer:** Resources, formal analysis, data curation, validation. **E. ten Hacken:** Resources, data curation, formal analysis. **S. Parvin:** Validation, data curation, formal analysis. **F. Lucas:** Data curation, formal analysis. **M. Uduman:** Data curation, formal analysis. **C. Gutierrez:** Data curation. **N. Dangle:** Data curation. **L. Billington:** Data curation. **F.F. Regis:** Data curation. **L.Z. Rassenti:** Resources. **A. Mohammad:** Data curation. **G.B. Hoffmann:** Data curation. **K. Stevenson:** Formal analysis. **M. Zheng:** Resources. **E. Witten:** Data curation. **S.M. Fernandes:** Resources. **E. Tausch:** Resources. **C. Sun:** Resources. **S. Stilgenbauer:** Resources. **J.R. Brown:** Resources. **T.J. Kipps:** Resources. **J.C. Aster:** Resources. **A. Gnirke:** Resources. **D.S. Neuberg:** Formal analysis. **A. Letai:** Resources. **L. Wang:** Resources. **R.D. Carrasco:** Resources, data curation, formal analysis. **A. Meissner:** Resources. **C.J. Wu:** Conceptualization, resources, data curation, supervision, funding acquisition.

Acknowledgments

The authors thank the members of the Wu lab, in particular Drs. Erin Parry and Satyen Gohil for their valuable feedback and critical insights. The authors are also grateful for the DFCI Animal Research Facility technical team and Flow Cytometry Core for truly excellent technical support, and the Dana-Farber/Harvard Cancer Center in Boston, MA, for the use of the Specialized Histopathology Core. Dana-Farber/Harvard Cancer Center is supported in part by an NCI Cancer Center Support Grant (NIH 5 P30 CA06516). The authors are also grateful to Binyamin Knisbacher, Cynthia Hahn, J.C. Aster, Oriol Olive, Adrian Wiestner, and Tuan Tran for their generous support. This study was supported by grants from the NIH/NCI (P01 CA206978, P01-CA081534, R01CA216273, and UG1CA233338). This work was further supported in part by the Lymphoma Research Foundation (A. Biran) and the Leukemia & Lymphoma Society (A. Biran). A. Biran is an Awardee of the Weizmann Institute of Science—Israel National Postdoctoral Award Program for Advancing

Women in Science. E. ten Hacken is a Scholar of the American Society of Hematology. A. Mohammad is supported by the Max Planck Society. C. Sun is supported by the Intramural Research Program of the National Heart, Lung, and Blood Institute, NIH. E. Tausch and S. Stilgenbauer received research support from DFG SFB1074 subproject B1 and B2. J.R. Brown is supported by NIH R01 CA 213442, P01 CA206978, and P01-CA081534.

The costs of publication of this article were defrayed in part by the payment of page charges. This article must therefore be hereby marked *advertisement* in accordance with 18 U.S.C. Section 1734 solely to indicate this fact.

Received April 22, 2021; revised August 18, 2021; accepted October 19, 2021; published first October 22, 2021.

References

1. Landau DA, Tausch E, Taylor-Weiner AN, Stewart C, Reiter JG, Bahlo J, et al. Mutations driving CLL and their evolution in progression and relapse. Nature 2015;526:525–30.
2. Wang L, Lawrence MS, Wan Y, Stojanov P, Sougnez C, Stevenson K, et al. SF3B1 and other novel cancer genes in chronic lymphocytic leukemia. N Engl J Med 2011;365:2497–506.
3. Yin S, Gambe RG, Sun J, Martinez AZ, Cartun ZJ, Regis FFD, et al. A murine model of chronic lymphocytic leukemia based on B cell-restricted expression of Sf3b1 mutation and atm deletion. Cancer Cell 2019;35:283–96.
4. Lazarian G, Yin S, ten Hacken E, Sewastianik T, Uduman M, Font-Tello A, et al. A hotspot mutation in transcription factor IKZF3 drives B cell neoplasia via transcriptional dysregulation. Cancer Cell 2021;39:380–93.
5. You JS, Jones PA. Cancer genetics and epigenetics: two sides of the same coin? Cancer Cell 2012;22:9–20.
6. Gaiti F, Chaligne R, Gu H, Brand RM, Kothen-Hill S, Schulman RC, et al. Epigenetic evolution and lineage histories of chronic lymphocytic leukaemia. Nature 2019;569:576.
7. Kulis M, Esteller M. DNA methylation and cancer. Adv Genet 2010;70:27–56.
8. Ehrlich M. DNA methylation in cancer: too much, but also too little. Oncogene 2002;21:5400–13.
9. Landau DA, Clement K, Ziller MJ, Boyle P, Fan J, Gu H, et al. Locally disordered methylation forms the basis of intratumor methylome variation in chronic lymphocytic leukemia. Cancer Cell 2014;26:813–25.
10. Kulis M, Heath S, Bibikova M, Queirós AC, Navarro A, Clot G, et al. Epigenomic analysis detects widespread gene-body DNA hypomethylation in chronic lymphocytic leukemia. Nat Genet 2012;44:1236–42.
11. Kretzmer H, Biran A, Purroy N, Lemvigh CK, Clement K, Gruber M, et al. Preneoplastic alterations define CLL DNA methylome and persist through disease progression and therapy. Blood Cancer Discov 2021;2:54–69.
12. Pei L, Choi JH, Liu J, Lee EJ, McCarthy B, Wilson JM, et al. Genome-wide DNA methylation analysis reveals novel epigenetic changes in chronic lymphocytic leukemia. Epigenetics 2012;7:567–78.
13. Lyko F. The DNA methyltransferase family: a versatile toolkit for epigenetic regulation. Nat Rev Genet 2018;19:81–92.
14. Bagacean C, Tempescul A, Le Dantec C, Bordron A, Mohr A, Saad H, et al. Alterations in DNA methylation/demethylation intermediates predict clinical outcome in chronic lymphocytic leukemia. Oncotarget 2017;8:65699–716.
15. Klein U, Lia M, Crespo M, Siegel R, Shen Q, Mo T, et al. The DLEU2/miR-15a/16–1 cluster controls B cell proliferation and its deletion leads to chronic lymphocytic leukemia. Cancer Cell 2010;17:28–40.
16. Guryanova OA, Lieu YK, Garrett-Bakelman FE, Spitzer B, Glass JL, Shank K, et al. Dnmt3a regulates myeloproliferation and liver-specific expansion of hematopoietic stem and progenitor cells. Leukemia 2016;30:1133–42.
17. Ryan JA, Brunelle JK, Letai A. Heightened mitochondrial priming is the basis for apoptotic hypersensitivity of CD4+ CD8+ thymocytes. Proc Natl Acad Sci U S A 2010;107:12895–900.
18. Dobin A, Davis CA, Schlesinger F, Drenkow J, Zaleski C, Jha S, et al. STAR: ultrafast universal RNA-seq aligner. Bioinformatics 2013;29:15–21.
19. Love MI, Huber W, Anders S. Moderated estimation of fold change and dispersion for RNA-seq data with DESeq2. Genome Biol 2014;15:550.
20. Scielzo C, Bertilaccio MTS, Simonetti G, Dagklis A, ten Hacken E, Fazi C, et al. HS1 has a central role in the trafficking and homing of leukemic B cells. Blood 2010;116:3537–46.
21. Martin M. Cutadapt removes adapter sequences from high-throughput sequencing reads. EMBnet J 2011;17:10–2.
22. Xi Y, Li W. BSMAP: whole genome bisulfite sequence MAPping program. BMC Bioinformatics 2009;10:232.
23. Sun D, Xi Y, Rodriguez B, Park HJ, Tong P, Meong M, et al. MOABS: model based analysis of bisulfite sequencing data. Genome Biol 2014;15:R38.
24. Jühling F, Kretzmer H, Bernhart SH, Otto C, Stadler PF, Hoffmann S. metilene: fast and sensitive calling of differentially methylated regions from bisulfite sequencing data. Genome Res 2016;26:256–62.
25. Bond J, Touzart A, Leprêtre S, Graux C, Bargetzi M, Lhermitte L, et al. DNMT3A mutation is associated with increased age and adverse outcome in adult T-cell acute lymphoblastic leukemia. Haematologica 2019;104:1617–25.
26. Lin ME, Hou HA, Tsai CH, Wu SJ, Kuo YY, Tseng MH, et al. Dynamics of DNMT3A mutation and prognostic relevance in patients with primary myelodysplastic syndrome. Clin Epigenetics 2018;10:42.
27. Bagacean C, Le Dantec C, Berthou C, Tempescul A, Saad H, Bordron A, et al. Combining cytogenetic and epigenetic approaches in chronic lymphocytic leukemia improves prognosis prediction for patients with isolated 13q deletion. Clin Epigenetics 2017;9:122.
28. Spencer DH, Russler-Germain DA, Ketkar S, Helton NM, Lamprecht TL, Fulton RS, et al. CpG island hypermethylation mediated by DNMT3A is a consequence of AML progression. Cell 2017;168:801–16.
29. Ryan RJH, Petrovic J, Rausch DM, Zhou Y, Lareau CA, Kluk MJ, et al. A B cell regulome links notch to downstream oncogenic pathways in small B cell lymphomas. Cell Rep 2017;21:784–97.
30. Tesi A, de Pretis S, Furlan M, Filipuzzi M, Morelli MJ, Andronache A, et al. An early Myc-dependent transcriptional program orchestrates cell growth during B-cell activation. EMBO Rep 2019;20:e47987.
31. Anderson MA, Deng J, Seymour JF, Tam C, Kim SY, Fein J, et al. The BCL2 selective inhibitor venetoclax induces rapid onset apoptosis of CLL cells in patients via a TP53-independent mechanism. Blood 2016;127:3215–24.
32. Ponader S, Chen S-S, Buggy JJ, Balakrishnan K, Gandhi V, Wierda WG, et al. The Bruton tyrosine kinase inhibitor PCI-32765 thwarts chronic lymphocytic leukemia cell survival and tissue homing in vitro and in vivo. Blood 2012;119:1182–9.
33. Mangolini M, Götte F, Moore A, Ammon T, Oelsner M, Lutzny-Geier G, et al. Notch2 controls non-autonomous Wnt-signalling in chronic lymphocytic leukaemia. Nat Commun 2018;9:3839.
34. Okano M, Bell DW, Haber DA, Li E. DNA Methyltransferases Dnmt3a and Dnmt3b are essential for de novo methylation and mammalian development. Cell 1999;99:247–57.
35. Challen GA, Sun D, Jeong M, Luo M, Jelinek J, Berg JS, et al. Dnmt3a is essential for hematopoietic stem cell differentiation. Nat Genet 2011;44:23–31.
36. Izzo F, Lee SC, Poran A, Chaligne R, Gaiti F, Gross B, et al. DNA methylation disruption reshapes the hematopoietic differentiation landscape. Nat Genet 2020;52:378–87.
37. Celik H, Mallaney C, Kothari A, Ostrander EL, Eultgen E, Martens A, et al. Enforced differentiation of Dnmt3a-null bone marrow leads to failure with c-Kit mutations driving leukemic transformation. Blood 2015;125:619–28.
38. Mayle A, Yang L, Rodriguez B, Zhou T, Chang E, Curry CV, et al. Dnmt3a loss predisposes murine hematopoietic stem cells to malignant transformation. Blood 2015;125:629–38.
39. Kramer AC, Kothari A, Wilson WC, Celik H, Nikitas J, Mallaney C, et al. Dnmt3a regulates T-cell development and suppresses T-ALL transformation. Leukemia 2017;31:2479–90.
40. Haney SL, Upchurch GM, Opavska J, Klinkebiel D, Hlady RA, Suresh A, et al. Promoter hypomethylation and expression is conserved in mouse chronic lymphocytic leukemia induced by decreased or inactivated Dnmt3a. Cell Rep 2016;15:1190–201.
41. Haney SL, Upchurch GM, Opavska J, Klinkebiel D, Appiah AK, Smith LM, et al. Loss of Dnmt3a induces CLL and PTCL with distinct methylomes and transcriptomes in mice. Sci Rep 2016;6:34222.
42. Peters SL, Hlady RA, Opavska J, Klinkebiel D, Pirruccello SJ, Talmon GA, et al. Tumor suppressor functions of Dnmt3a and Dnmt3b in the prevention of malignant mouse lymphopoiesis. Leukemia 2014;28:1138–42.

43. Mahajan VS, Mattoo H, Sun N, Viswanadham V, Yuen GJ, Allard-Chamard H, et al. B1a and B2 cells are characterized by distinct CpG modification states at DNMT3A-maintained enhancers. Nat Commun 2021;12:2208.
44. Ostrander EL, Kramer AC, Mallaney C, Celik H, Koh WK, Fairchild J, et al. Divergent effects of Dnmt3a and Tet2 mutations on hematopoietic progenitor cell fitness. Stem Cell Reports 2020;14:551.
45. Joseph C, Quach JM, Walkley CR, Lane SW, Lo Celso C, Purton LE. Deciphering hematopoietic stem cells in their niches: a critical appraisal of genetic models, lineage tracing, and imaging strategies. Cell Stem Cell 2013;13:520–33.
46. Meissner A, Gnirke A, Bell GW, Ramsahoye B, Lander ES, Jaenisch R. Reduced representation bisulfite sequencing for comparative high-resolution DNA methylation analysis. Nucleic Acids Res 2005;33:5868–77.